Neutrophils initiate the destruction of the olfactory epithelium during SARS-CoV-2 infection in hamsters

Bourgon Clara, St Albin Audrey, Ando-Grard Ophélie, Da Costa Bruno, Domain Roxane, Korkmaz Brice, Klonjkowski Bernard, Le Poder Sophie, Meunier Nicolas

▶ **To cite this version:**

Bourgon Clara, St Albin Audrey, Ando-Grard Ophélie, Da Costa Bruno, Domain Roxane, et al.. Neutrophils initiate the destruction of the olfactory epithelium during SARS-CoV-2 infection in hamsters. 2024. hal-04494758

HAL Id: hal-04494758
https://hal.uvsq.fr/hal-04494758

Preprint submitted on 7 Mar 2024

HAL is a multi-disciplinary open access archive for the deposit and dissemination of scientific research documents, whether they are published or not. The documents may come from teaching and research institutions in France or abroad, or from public or private research centers.

L'archive ouverte pluridisciplinaire **HAL**, est destinée au dépôt et à la diffusion de documents scientifiques de niveau recherche, publiés ou non, émanant des établissements d'enseignement et de recherche français ou étrangers, des laboratoires publics ou privés.

bioRxiv preprint doi: https://doi.org/10.1101/2022.03.15.484439; this version posted March 15, 2022. The copyright holder for this preprint (which was not certified by peer review) is the author/funder, who has granted bioRxiv a license to display the preprint in perpetuity. It is made available under aCC-BY-NC-ND 4.0 International license.

1 **Neutrophils initiate the destruction of the olfactory epithelium during SARS-CoV-2 infection in**
2 **hamsters**

3 Bourgon Clara[1], St Albin Audrey[1], Ando-Grard Ophélie [1], Da Costa Bruno[1], Domain Roxane[2], Korkmaz
4 Brice[2], Klonjkowski Bernard[3], Le Poder Sophie[3], Meunier Nicolas[1]

5 [1]Unité de Virologie et Immunologie Moléculaires (UR892), INRAE, Université Paris-Saclay, Jouy-en-
6 Josas, France

7 [2]INSERM UMR-1100, “Research Center for Respiratory Diseases” and University of Tours, 37032
8 Tours, France

9 [3]UMR 1161 Virologie, INRAE-ENVA-ANSES, École Nationale Vétérinaire d'Alfort, Maisons-Alfort,
10 94704 Paris, France

11 # Abstract

12 The loss of smell related to SARS-CoV-2 infection is one of the most prevalent symptoms of COVID-19.
13 It is now clear that this symptom is related to the massive infection by SARS-CoV-2 of the olfactory
14 epithelium leading to its desquamation. However, the molecular mechanism behind the
15 destabilization of the olfactory epithelium is less clear. Using golden Syrian hamster, we show here
16 that while apoptosis remains at a low level in damaged infected epithelium, the latter is invaded by
17 innate immunity cells. By depleting the neutrophil population or blocking the activity of neutrophil
18 elastase-like proteinases, we reduced the damage induced by the SARS-CoV-2 infection. Surprisingly,
19 the impairment of neutrophil activity led to a decrease of SARS-CoV-2 infection levels in the nasal
20 cavity. Our results indicate a counterproductive role of neutrophils leading to the release of infected
21 cells in the lumen of the nasal cavity and thereby enhanced spreading of the virus.

22 **Abbreviations**: OE (olfactory epithelium), OSN (olfactory sensory neuron), SCs (sustentacular cells),
23 MPO (myeloperoxidase), neutrophil, proteases.

bioRxiv preprint doi: https://doi.org/10.1101/2022.03.15.484439; this version posted March 15, 2022. The copyright holder for this preprint (which was not certified by peer review) is the author/funder, who has granted bioRxiv a license to display the preprint in perpetuity. It is made available under aCC-BY-NC-ND 4.0 International license.

24 ## Introduction

25 Loss of smell (anosmia) is a major symptom of COVID-19 pandemic. With omicron's increased
26 transmission, hundreds of thousands of people per day still get infected worldwide. Despite omicron's
27 reduced anosmia prevalence (UK Health Security Agency Technical Briefing Jan 14, 2022), loss of smell
28 will likely affect millions more (Vaira et al., 2021; von Bartheld et al., 2020) and 10% of anosmic patients
29 might not recover their sense of smell 6 months after the disease onset (*3*, *4*). The full olfactory
30 recovery could even take up to one year and some patients may never recover their sense of smell (*5*).
31 A recent study estimates that in the US about 720,000 people actually suffer from chronic olfactory
32 disorder related to COVID-19 (*6*). The loss of smell negatively impacts life quality by disrupting feeding
33 behavior potentially leading to malnutrition; and by exposing to food poisoning and to inhalation of
34 dangerous chemicals (*7*). In severe and persistent cases, anosmic patients could possibly suffer from
35 chronic depression (*8*). It is thus crucial to understand the cellular basis of anosmia.

36 Olfaction starts in the olfactory epithelium (OE) which contains olfactory sensory neurons (OSNs)
37 surrounded by supporting cells called sustentacular cells (SCs). Both cell types are regenerated
38 regularly due to multipotent basal cells (*9*). Among these cells, only SCs express significantly ACE2 and
39 TRPMSS2 required for SARS-CoV-2 cellular entrance (*10*–*12*). In a previous study, we observed in the
40 golden Syrian hamster model that SARS-CoV-2 infects massively the sustentacular cells in the OE
41 leading to its desquamation and olfactory neurons loss (Bryche et al., 2020). Although very rarely OSNs
42 may be infected by SARS-CoV-2 (*15*), a recent study in humans concludes that anosmia arises primarily
43 from infection of sustentacular cells of the OE followed by the disruption of OE integrity without OSN
44 infection (Khan et al., 2021b).

45 Previous studies in rodents have concluded that more than 90% of the OE needs to be destroyed to
46 impair olfactory-mediated food-finding behaviour (*16*). This suggests that a large area of the OE has to
47 become dysfunctional to experience anosmia in COVID-19. How does SARS-CoV-2 achieve such an
48 unprecedented success in dismantling the sense of smell, compared with previous coronavirus and
49 influenza pandemics? Several studies reported that most cells of the infected OE including OSNs
50 undergo apoptosis (*17*–*20*) leading to desquamation. A similar phenomenon has been reported during
51 influenza infection (*21*) and has been considered for SARS-CoV-2 as a defence mechanism to limit a
52 potential invasion of the central nervous system by pathogens using the olfactory route (*22*).
53 Alternatively, innate immune cells could trigger directly the desquamation of the OE through
54 inflammation as observed in the lung (*23*). Indeed, innate immune cells invade massively the SARS-
55 CoV-2 infected OE (*13*). Iba1 is a marker of microglia/macrophages (*24*) which are the most studied
56 innate immunity cells in the nasal cavity (*21*). Iba1^{+} microglial cells ensure viral clearance by

bioRxiv preprint doi: https://doi.org/10.1101/2022.03.15.484439; this version posted March 15, 2022. The copyright holder for this preprint (which was not certified by peer review) is the author/funder, who has granted bioRxiv a license to display the preprint in perpetuity. It is made available under aCC-BY-NC-ND 4.0 International license.

57 phagocytizing viral particles and infected cells (*25*, *26*) and can induce cell death as observed in the
58 hippocampus using the Theiler's virus model of encephalitis (*27*). As the OE is not protected by the
59 blood brain barrier, neutrophils and monocytes/macrophages classically recruited during the early
60 event of inflammation could also be involved in the OE damage following SARS-CoV-2 infection (*28*,
61 *29*). Neutrophils are well known for their ability to induce tissue damage, notably through the release
62 of elastase-like proteinases (*30*, *31*) as well as the production of reactive oxygen species (ROS) by the
63 myeloperoxidase (MPO) and formation of toxic neutrophil extracellular traps (*32*, *33*). Macrophages
64 are known for their ability to phagocyte pathogens, produce cytokines and activate other immune cells
65 (*34*). Although they are involved in the regeneration of the OE (*35*, *36*), they can also lead to tissue
66 damage during viral infections notably through NLRP3 inflammasome activation and
67 metalloproteinases activity (*29*). In this study, we focused on the early events following SARS-CoV-2
68 infection of the nasal cavity to explore the mechanism of the unusually extensive OE damage following
69 SARS-CoV-2 infection.

70 ## Material and methods

71 **Study design**

72 The study was performed to understand the cellular mechanisms leading to the SARS-CoV-2 induced
73 damage in the OE using hamsters as an animal model. Hamsters experiments were planned in
74 accordance with the principles of the 3Rs (replacement, reduction, and refinement). Body weight and
75 animal behaviour was monitored before and during the experiments. Different parameters in the nasal
76 cavity were measured by quantitative polymerase chain reaction (qPCR) and by
77 immunohistochemistry. Leucocyte numeration was performed directly by an automated analyser.
78 SARS-CoV-2 replication was measured *in vitro* to evaluate a potential inhibition by the drugs used to
79 modulate neutrophils activity. Sample size for each experiment is indicated in figure legends. During
80 analysis, all data points were included except because of technical failure to process the sample.
81 Animals were randomized to the experimental groups. All analyses were performed blindly of the
82 treatment.

83 **SARS-CoV-2 isolates**

84 Experiments were carried out with SARS-CoV-2 strain BetaCoV/France/IDF/200107/2020, which was
85 isolated by Dr. Paccoud from the La Pitié-Salpétrière Hospital in France. This strain was kindly provided
86 by the Urgent Response to Biological Threats (CIBU) hosted by Institut Pasteur (Paris, France), headed
87 by Dr. Jean-Claude Manuguerra. Cell culture experiments were performed with the SARS-CoV-2 strain
88 France/IDF0372/2020 kindly provided by Sylvie van der Werf.

bioRxiv preprint doi: https://doi.org/10.1101/2022.03.15.484439; this version posted March 15, 2022. The copyright holder for this preprint (which was not certified by peer review) is the author/funder, who has granted bioRxiv a license to display the preprint in perpetuity. It is made available under aCC-BY-NC-ND 4.0 International license.

89 **Animals**

90 Fifty-six 8 weeks-old male hamsters were purchased from Janvier's breeding Center (Le Genest, St Isle,
91 France). Animal experiments were carried out in the animal biosafety level 3 facility of the UMR
92 Virologie (ENVA, Maisons-Alfort); approved by the ANSES/EnvA/UPEC Ethics Committee (CE2A16) and
93 authorized by the French ministry of Research under the number APAFIS#25384-2020041515287655.
94 Infection was achieved by nasal instillation (40 µL in each nostril with 5.10^3 $TCID_{50}$ of SARS-CoV2 strain
95 BetaCoV/France/IDF/200107/2020) on anesthetised animals under isofluorane. Seven mock-infected
96 animals received only Dulbecco's minimal essential medium.
97 For neutrophil depletion experiments, hamsters were injected intraperitoneally with either PBS or 150
98 mg/kg and 100 mg/kg of cyclophosphamide (CAS: 6055-19-2; PHR1404; Sigma Aldrich) at 3 and 1 days
99 before SARS-CoV-2 infection. Half of the animals were sacrificed at 1 dpi (days post infection) and the
100 other half at 2 dpi (n=4 in each group).
101 To inhibit neutrophil elastase-like proteases, we used a synthetic cathepsin C inhibitor ($IcatC_{XPZ-01}$; (*37*)
102 diluted in 10 % (2-Hydroxypropyl)-β-cyclodextrin (CAS : 128446-35-5; C0926; Sigma-Aldrich)
103 suspended in citrate buffer 50 mM at pH=5 (vehicle) as described previously (*38*). Hamsters were
104 injected intraperitoneally twice a day with either vehicle (n=4) or $Icat_{CXPZ-01}$ at 4.5 mg/kg for 10 days
105 before infection by SARS-CoV-2 (n=4). Animals were sacrificed at 1 dpi.
106 For all experiments except $IcatC_{XPZ-01}$ treatment, the head was divided sagitally into two halves, of
107 which one was used for immunohistochemistry experiments. Nasal turbinates were extracted from
108 the other half for qPCR analysis. Only histological analysis was performed on tissues from $IcatC_{XPZ-01}$
109 treatment experiments.

110 **Immunohistochemistry and quantifications**

111 The immunohistochemistry analysis of the olfactory mucosa tissue sections was performed as
112 described previously in mice (*39*). Briefly, the animal hemi-heads were fixed for 3 days at room
113 temperature in 4% paraformaldehyde (PFA) and decalcified in Osteosoft (Osteosoft; 101728; Merck
114 Millipore; Saint-Quentin Fallavier; France) for 3 weeks. Blocks were cryo-protected in 30% sucrose.
115 Cryo-sectioning (12 µm) was performed in coronal sections of the nasal cavity, perpendicular to the
116 hard palate in order to examine the vomeronasal organ (VNO), olfactory epithelium (OE), Steno's gland
117 and olfactory bulb. Sections were stored at -80 °C until use.
118 Non-specific staining was blocked by incubation with 2% bovine serum albumin (BSA) and 0.05%
119 Tween. The sections were then incubated overnight with primary antibodies directed against SARS
120 Nucleocapsid protein (1/500 ; mouse monoclonal ; clone 1C7C7 ; Sigma-Aldrich), ionised calcium-
121 binding adapter molecule 1 (Iba1) (1/500 ; rabbit monoclonal ; clone EPR16588 ; Abcam),
122 myeloperoxidase protein (MPO) (1/500 ; rabbit monoclonal ; clone EPR20257 ; Abcam), CD68 (1/200 ;

bioRxiv preprint doi: https://doi.org/10.1101/2022.03.15.484439; this version posted March 15, 2022. The copyright holder for this preprint (which was not certified by peer review) is the author/funder, who has granted bioRxiv a license to display the preprint in perpetuity. It is made available under aCC-BY-NC-ND 4.0 International license.

123 rabbit polyclonal; PA1518; Boster), cleaved caspase 3 (C3C) (1/200 ; rabbit polyclonal ; #9661 ; Cell
124 signalling), G_{olf} (1/300 ; rabbit polyclonal ; C-18 ; Santa Cruz) and Olfactory Marker Protein (OMP)
125 (1/500 ; goat polyclonal ; 544-10001, Wako). Fluorescence staining was performed using goat anti-
126 mouse-A555; goat anti-rabbit-A488 and donkey anti-goat-A546 (1/800; Molecular Probes A21422;
127 A11056; A11008 respectively; Invitrogen; Cergy-Pontoise; France).
128 Images were taken at x100 magnification using a 1X71 Olympus microscope equipped with an Orca ER
129 Hamamatsu cooled CCD camera (Hamamatsu Photonics France; Massy; France). Whole section images
130 were taken at x50 magnification using a Leica MZ10F Fluorescent binocular microscope.
131 To assess olfactory epithelium damage, we used a global score from 1 to 9 based on the integrity of
132 the OE. To evaluate the correlation of apoptosis and innate immune cell presence with damage, OE
133 areas were divided in two groups: undamaged areas (damage score equal to 1 or 2) and damaged areas
134 (damage score between 5 and 9). Apoptosis level, infiltration of immune cells in the OE and its
135 underlying lamina propria were quantified as the percentage of the area positive for C3C (cleaved
136 caspase 3); Iba1 (macrophages/microglia), CD68 (activated bone-marrow-derived macrophages) and
137 MPO (neutrophils). For each animal, the percentage of stained OE was averaged over 4 distinct areas
138 in the beginning of olfactory turbinates at 1 dpi and in the medial part of the nasal cavity containing
139 Steno's gland and NALT at 2 dpi.
140 In cyclophosphamide and in $IcatC_{XPZ-01}$ experiments, we examined two independent sections of nasal
141 turbinates (separated by 500 µm) in the middle of the nasal cavity containing NALT and Steno's gland.
142 For each section, we set a global score from 1 to 9 for neutrophil infiltration based on the overall
143 presence of MPO signal in nasal mucosa and in nasal cavity lumen. For each section, we also measured
144 the total infected area of the OE, the area of desquamated cells in the lumen (based on Hoechst nuclear
145 staining) and the percentage of infected desquamated cells in the lumen (based on N protein
146 immunostaining).
147 All quantifications were made with ImageJ (Rasband, W.S., ImageJ, U.S. National Institutes of Health,
148 Bethesda, Maryland, USA, http://imagej.nih.gov/ij/, 1997–2012) to threshold specific staining.

149 **RNA extraction and RT-qPCR analysis**

150 Total RNA was extracted from frozen nasal turbinates using the Trizol-chloroforme method as
151 described previously (*39*). Oligo-dT first strand cDNA synthesis was performed from 5 µg total RNA
152 with iScript Advance cDNA Synthesis Kit for RT-qPCR (Bio-Rad; #1725038) following manufacturer's
153 recommendations. qPCR was carried out using 125 ng of cDNA added to a 15 µL reaction mix. This
154 reaction mix contained 10 µL iTaq Universal Sybr Green SuperMix (BioRad; #1725124), and primers at
155 500 nM (sequences in **Supp. Table 1)**. The reaction was performed with a thermocycler (Mastercycler
156 ep Realplex, Eppendorf). Fluorescence during qPCR reaction was monitored and measured by Realplex

bioRxiv preprint doi: https://doi.org/10.1101/2022.03.15.484439; this version posted March 15, 2022. The copyright holder for this preprint (which was not certified by peer review) is the author/funder, who has granted bioRxiv a license to display the preprint in perpetuity. It is made available under aCC-BY-NC-ND 4.0 International license.

157 Eppendorf software. A dissociation curve was plotted at the end of the fourty amplification cycles of
158 the qPCR to check the ability of theses primers to amplify a single and specific PCR product.
159 Quantification of initial specific RNA concentration was done using the *ΔΔCt* method. Standard controls
160 of specificity and efficiency of the qPCR were performed. The mRNA expression of each gene was
161 normalized with the expression level of G3PDH. A correction factor was applied to each primer pair
162 according to their efficiency (*40*).

163 **Measure of antiviral activity of cyclophosphamide and cathepsin C inhibitor against SARS-CoV-2 in**
164 **cell culture**

165 Vero E6 cells (CRL-1586, ATCC maintained at 37 °C; 5% CO_2) were seeded at 2.10^4 cells per well in a 96-
166 well plate in Dulbecco's Modified Eagle's Medium, 5% foetal bovine serum (FBS-12A, Capricorn
167 Scientific, Cliniscience). For cyclophosphamide antiviral activity evaluation, cells were treated with
168 0.15 mg/mL (corresponding to the maximum dose potentially present in hamsters) or 0.45 mg/mL
169 cyclophosphamide diluted in sterile PBS. For $IcatC_{XPZ-01}$ antiviral activity evaluation, cells were treated
170 with 4.5 µg/mL (corresponding to the maximum dose potentially present in hamsters) or 13.5 µg/mL
171 $IcatC_{XPZ-01}$ diluted in 10% dextrin, citrate buffer 50 mM, pH=5. Cells were treated with vehicle as control
172 (n=6 for each condition). All treatments were performed one hour prior to infection with SARS-CoV-2
173 strain France/IDF0372/2020 at 5.10^3 pfu per well diluted in DMEM, 10% Fetal Bovine Serum. Loss of
174 cell viability reflecting the efficiency of viral infection was measured 3 days after infection by adding
175 100 µL Cell Titer-Glo reagent to each well (CellTiterGlo Luminescent Cell Viability Assay, Promega
176 #G7571), according to the manufacturer's protocol. Cell luminescence of each well was then quantified
177 using an Infinite M200Pro TECAN.

178 **Statistical analysis**

179 All comparisons were made using Prism 5.0 (GraphPad). Statistical significance between groups was
180 assessed using non-parametric Mann Whitney tests. For correlation analyses, we used Spearman
181 non-parametric test. Error bars indicate the SEM. Detailed information on statistical test used,
182 sample size and P value are provided in the figure legends.

bioRxiv preprint doi: https://doi.org/10.1101/2022.03.15.484439; this version posted March 15, 2022. The copyright holder for this preprint (which was not certified by peer review) is the author/funder, who has granted bioRxiv a license to display the preprint in perpetuity. It is made available under aCC-BY-NC-ND 4.0 International license.

183 # Results

184 **Apoptosis occurs after cell desquamation following SARS-CoV-2 infection of the olfactory**
185 **epithelium**

186 We previously observed that as soon as two days following nasal instillation of SARS-CoV-2 in Syrian
187 gold hamsters, the sustentacular cells of the olfactory epithelium were massively infected along with
188 strong cellular loss and cellular debris filling the lumen of the nasal cavity (*13*). In order to understand
189 the events leading to this desquamation, we chose to focus on the early stages of infection at 1 and 2
190 dpi. To evaluate the importance of apoptosis in the damage of the olfactory epithelium following SARS-
191 CoV-2 infection, we measured the level of cleaved caspase 3 signal in uninfected animals, and in
192 infected zones of the OE that were either intact or damaged (**Fig. 1**). Basal level of apoptosis occurring
193 in the OE was not increased in either zone at 1 or 2 dpi (**Fig. 1D**). However, we observed a strong
194 cleaved caspase 3 signal co-localizing partly with desquamated cell in the lumen of the nasal cavity.
195 The cleaved caspase 3 signal in the lumen of the nasal cavity was increased 5- and 14-fold compared
196 to the OE at 1 and 2 dpi respectively, which was statistically significant at 2 dpi (Mann Whitney,
197 p=0.0286) and nearly significant at 1 dpi (p=0.0525).

bioRxiv preprint doi: https://doi.org/10.1101/2022.03.15.484439; this version posted March 15, 2022. The copyright holder for this preprint (which was not certified by peer review) is the author/funder, who has granted bioRxiv a license to display the preprint in perpetuity. It is made available under aCC-BY-NC-ND 4.0 International license.

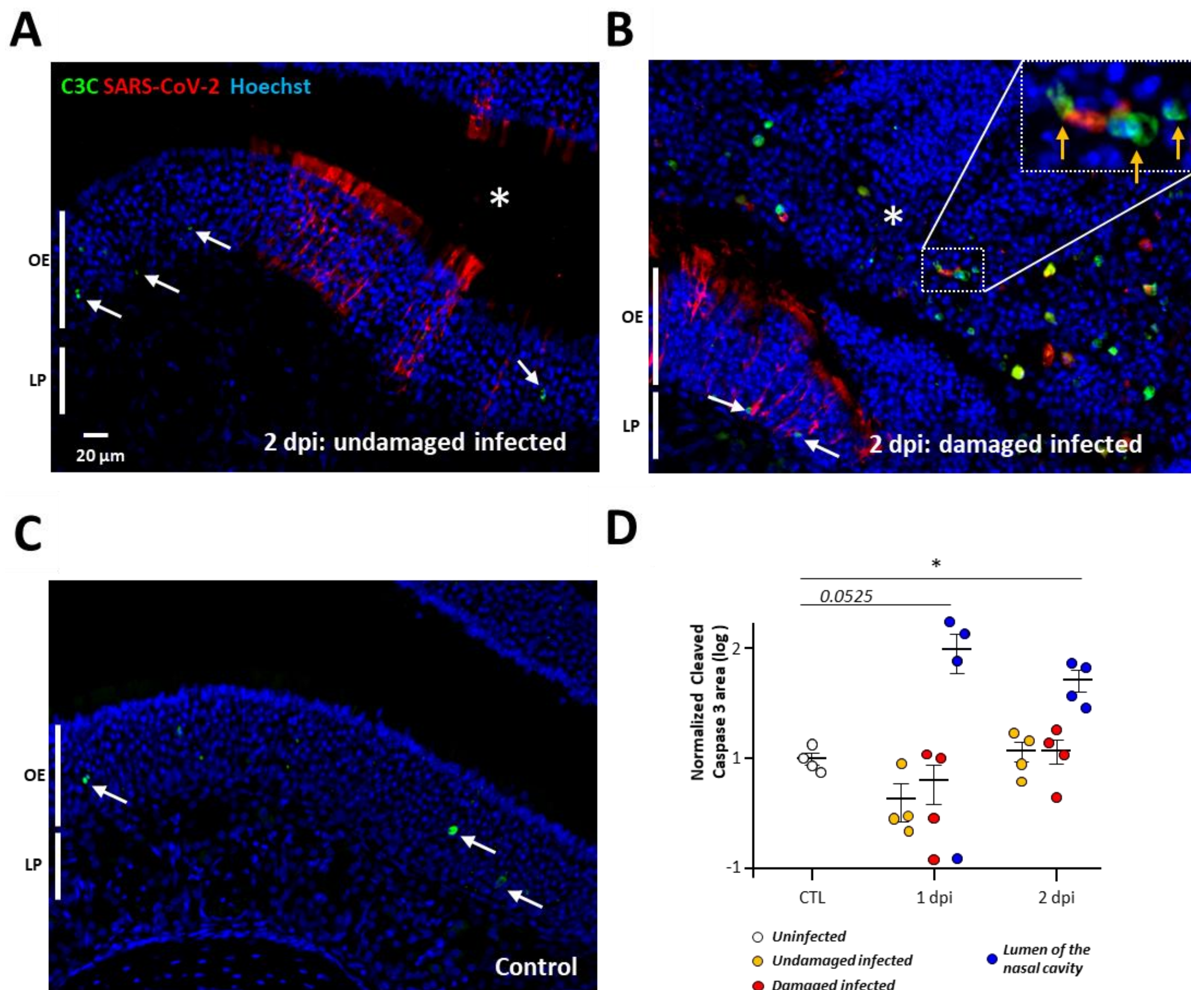

Figure 1: Apoptosis occurs in desquamated cells in the lumen of the nasal cavity following SARS-CoV-2 infection but not in the olfactory epithelium*. Representative images of an infected intact (**A**), infected damaged (**B**) and non (**C**) infected area of the olfactory epithelium at 2 days post infection (dpi). Apoptotic cells in the olfactory epithelium are indicated by a white arrow (OE; Olfactory Epithelium / LP Lamina Propria). The lumen of the nasal cavity is indicated by a white asterisk and is filled with cells some of which colocalize in their nucleus cleaved caspase 3 signal (orange arrow). (**D**) Cleaved caspase 3 signal in the olfactory epithelium normalized to control (log 10, Mean ± SEM, n=4, *p<0.01 (Mann-Whitney test)).*

198 **Damage of the infected olfactory epithelium is correlated with infiltration of innate immune cells**

199 Since apoptosis does not significantly occur in the OE during the initial phase of infection, the
200 desquamation of the infected OE may be related to immune cell infiltration (Bryche et al., 2020; Urata
201 et al., 2021). So far, the immune cells in the nasal cavity have been poorly characterized. Neutrophils
202 and macrophages are known for their importance in clearing infected tissue (*41*) but only Iba1^{+} cells

bioRxiv preprint doi: https://doi.org/10.1101/2022.03.15.484439; this version posted March 15, 2022. The copyright holder for this preprint (which was not certified by peer review) is the author/funder, who has granted bioRxiv a license to display the preprint in perpetuity. It is made available under aCC-BY-NC-ND 4.0 International license.

203 are well characterized in the OE (*21*). Iba1+ cells are described as microglia/macrophages but CD68 is
204 more classically used as a marker of monocytes and macrophages (*42*). Concerning neutrophils, the
205 presence of neutrophil cytosol factor 2 (ncf2; (*43*)) and myeloperoxydase (MPO) have been used
206 successfully to characterize these cells in hamsters (*44*).

207 We first evaluated at 1 dpi and 2 dpi by qPCR the expression of Iba1, CD68 and Ncf2 along with classical
208 inflammatory markers (TNFα and IL6) and the presence of the virus (**Supp. Fig 1**). At 1 dpi, SARS
209 Nucleocapsid protein (SARS N) was already abundantly expressed in the OE at a similar level as at 2
210 dpi, and TNFα and IL6 transcripts increased gradually (Mann-Whitney, $p<0.05$). Iba1 and CD68
211 expression related to macrophage presence in the OE did not rise significantly at 1 dpi compared to
212 control (Mann-Whitney, $p=0.164$ and *0.128* respectively) but did at 2 dpi (Mann-Whitney, $p<0.05$).
213 Concerning neutrophils, ncf2 expression was strongly enhanced at 1 dpi and was still increasing at 2
214 dpi (Mann-Whitney, $p<0.05$). These results suggest that neutrophils are already recruited at 1 dpi and
215 that their recruitment continues at 2 dpi along with the arrival of Iba1+ and CD68+ cells.

216 We next focused on immunostaining to characterize the presence of Iba1+, CD68+ and MPO+ cells. In
217 the OE of an uninfected hamster, Iba1+ cells were already present and mainly localized in the lamina
218 propria while CD68 signal was absent (**Fig. 2A**) indicating that Iba1+ cells do not express the classical
219 CD68 marker of macrophages. This was confirmed in the infected areas of the OE where we observed
220 a very different presence of Iba1+ and CD68+ cells. Iba1+ cells were massively present as soon as 1 dpi
221 in the damaged parts of the infected OE as well as in the desquamated cells in the lumen of the nasal
222 cavity. CD68+ cells were less abundant in the damaged part of the OE and mainly present in the
223 desquamated cells filling the lumen of the nasal cavity (**Fig. 2B**). A double staining against Iba1 and
224 CD68 of the desquamated cells in the lumen of the nasal cavity did not reveal any overlap of the two
225 markers (**Supp. Fig. 2)**, showing that Iba1+ cells do not express CD68 once they are located among the
226 desquamated cells. Similar to CD68, MPO signal was absent in uninfected OE and appears partly in the
227 damaged OE and mainly in the lumen of the nasal cavity along with desquamated cells. Overall, these
228 results show that Iba1+ microglia are much more abundant in the infected OE than CD68+ macrophages
229 and MPO+ neutrophils cells, both being mainly present in the desquamated cells filling the lumen of
230 the SARS-CoV-2 infected nasal cavity.

231

bioRxiv preprint doi: https://doi.org/10.1101/2022.03.15.484439; this version posted March 15, 2022. The copyright holder for this preprint (which was not certified by peer review) is the author/funder, who has granted bioRxiv a license to display the preprint in perpetuity. It is made available under aCC-BY-NC-ND 4.0 International license.

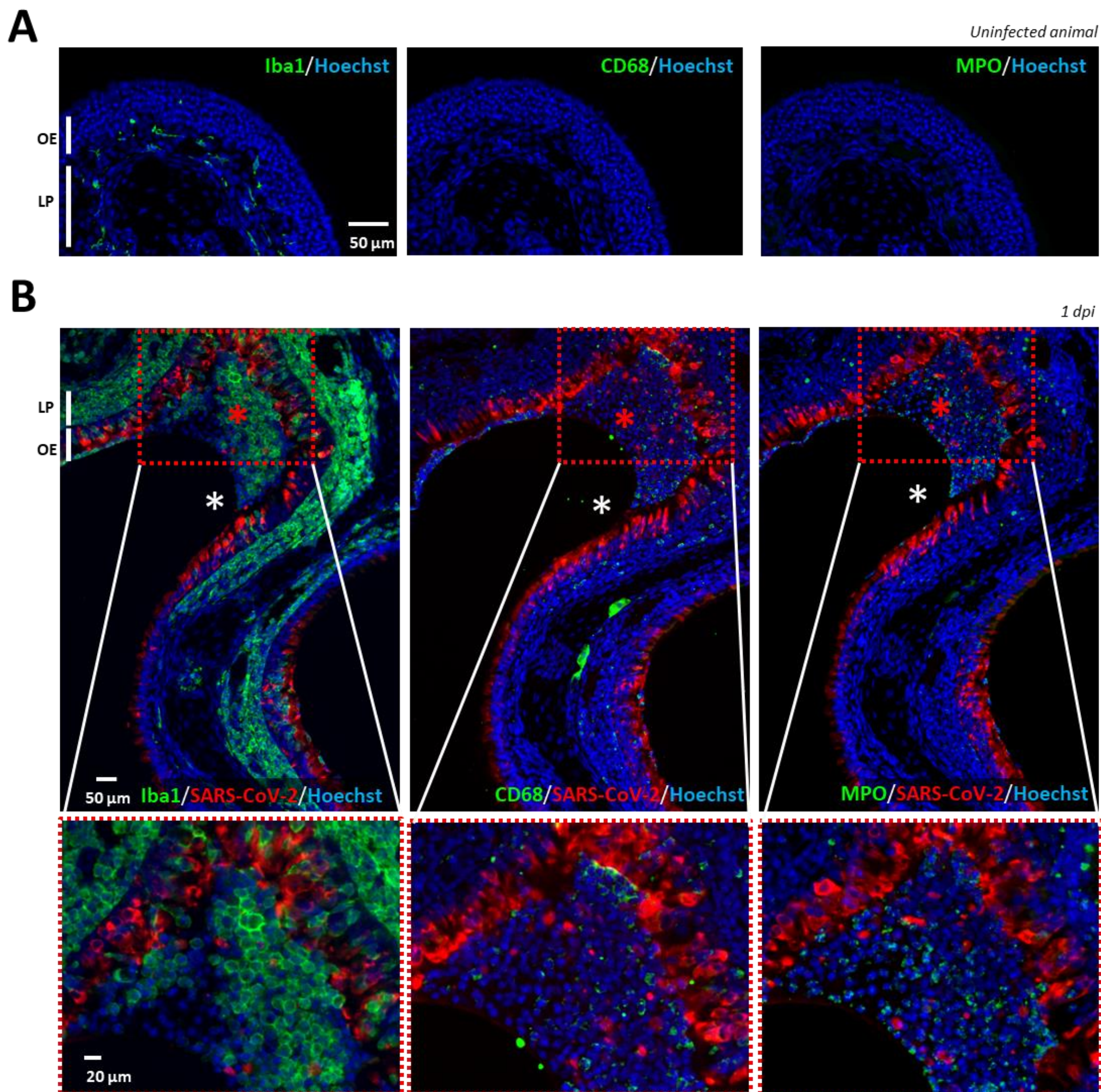

Figure 2: Iba1⁺ (microglia), CD68⁺ (macrophages) and MPO⁺ (neutrophils) cells presence in the olfactory epithelium before and during SARS-CoV-2 infection. *Immunostaining on successive slides of the olfactory epithelium from a non-infected (**A**) or 1 dpi hamster (**B**). Only Iba1⁺ cells are present in the uninfected olfactory epithelium (OE) and in the lamina propria (LP). In the infected epithelium, Iba1⁺ cells are massively present in the OE while CD68⁺ and MPO cells are mostly present in the desquamated cells (red asterisk) in the lumen of the nasal cavity (white asterisk).*

232

233 If these innate immunity cells are involved in the desquamation of the OE, we should always observe
234 their presence in the damaged infected area of the OE. To investigate their infiltration in the OE and
235 its correlation with damage, we focused on 3 zones similarly as for apoptosis quantification:
236 $^{1/}$uninfected, infected $^{2/}$without or $^{3/}$with damage at 1 and 2 dpi. The infiltration level of Iba1⁺ cells in

bioRxiv preprint doi: https://doi.org/10.1101/2022.03.15.484439; this version posted March 15, 2022. The copyright holder for this preprint (which was not certified by peer review) is the author/funder, who has granted bioRxiv a license to display the preprint in perpetuity. It is made available under aCC-BY-NC-ND 4.0 International license.

237 the OE was increased in the damaged infected zone but not in the undamaged one (**Fig. 3**). This
238 difference was statistically significant at 2 dpi (Mann-Whitney, *p= 0.0286*) and nearly significant at 1
239 dpi (*p= 0.0525*). The infiltration of these cells was similarly increased in the lamina propria underneath
240 the previous OE zones with a significant difference at 2 dpi (*p= 0.0286*). We observed a significant
241 correlation between the damage of the OE and their presence in both the OE and the underlying lamina
242 propria (Spearman test, *p = 0.0098* and *0.0006* respectively).

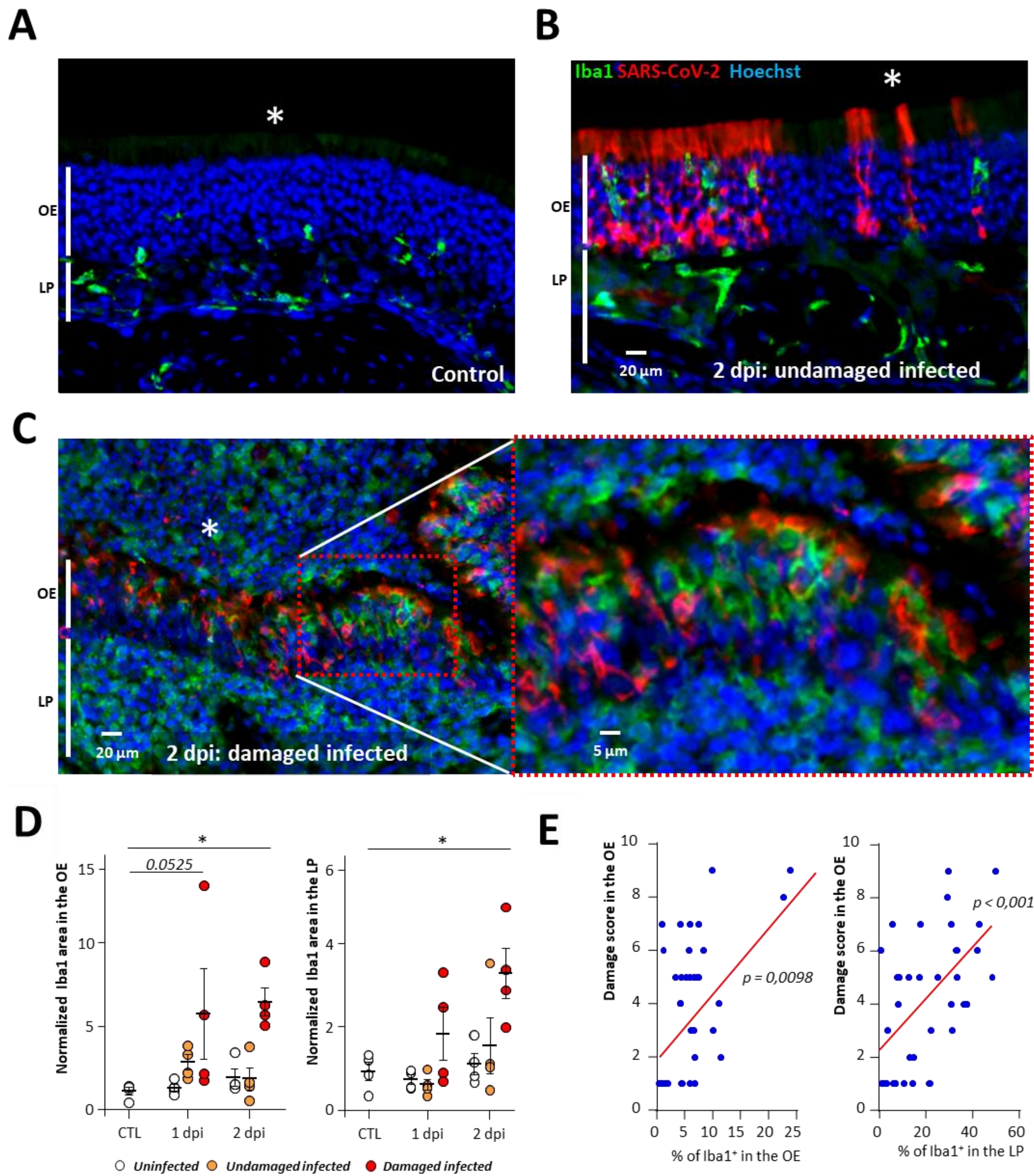

bioRxiv preprint doi: https://doi.org/10.1101/2022.03.15.484439; this version posted March 15, 2022. The copyright holder for this preprint (which was not certified by peer review) is the author/funder, who has granted bioRxiv a license to display the preprint in perpetuity. It is made available under aCC-BY-NC-ND 4.0 International license.

Figure 3: Iba1⁺ cell infiltration increases with the damage in the OE. *Representative images of uninfected (**A**), infected but undamaged (**B**) and infected and damaged (**C**) area of the olfactory epithelium (OE) at 2 days post infection (dpi). The lumen of the nasal cavity is indicated by a white asterisk. (**D**) $Iba1^+$ signal in the olfactory epithelium (OE, left) and lamina propria (LP, right) in either control animals (CTL) or at 1 or 2 dpi (Mean normalized to control ± SEM, n=4, *$p<0.01$ (Mann-Whitney test)). (**E**) Correlation between score damage of the olfactory epithelium and the percentage of $Iba1^+$ signal in the olfactory epithelium (left panel) and the lamina propria (right panel). Spearman test p value.*

243 We similarly examined whether the presence of $CD68^+$ macrophages and MPO^+ neutrophils in the OE
244 was associated with the damage of the OE after SARS-CoV-2 infection. Both CD68 and MPO signals
245 were increased in the damaged infected zone but not in the undamaged one (**Fig. 4**). This difference
246 was statistically significant in the infected damaged zones at 1 and 2 dpi for both markers compared
247 to control and infected undamaged zones of the OE and lamina propria (Mann-Whitney, $p< 0.05$). We
248 observed a significant correlation between the damage of the OE and their presence the presence of
249 both $CD68^+$ and MPO^+ cells the OE and the lamina propria (Spearman test, $p <0.001$).

bioRxiv preprint doi: https://doi.org/10.1101/2022.03.15.484439; this version posted March 15, 2022. The copyright holder for this preprint (which was not certified by peer review) is the author/funder, who has granted bioRxiv a license to display the preprint in perpetuity. It is made available under aCC-BY-NC-ND 4.0 International license.

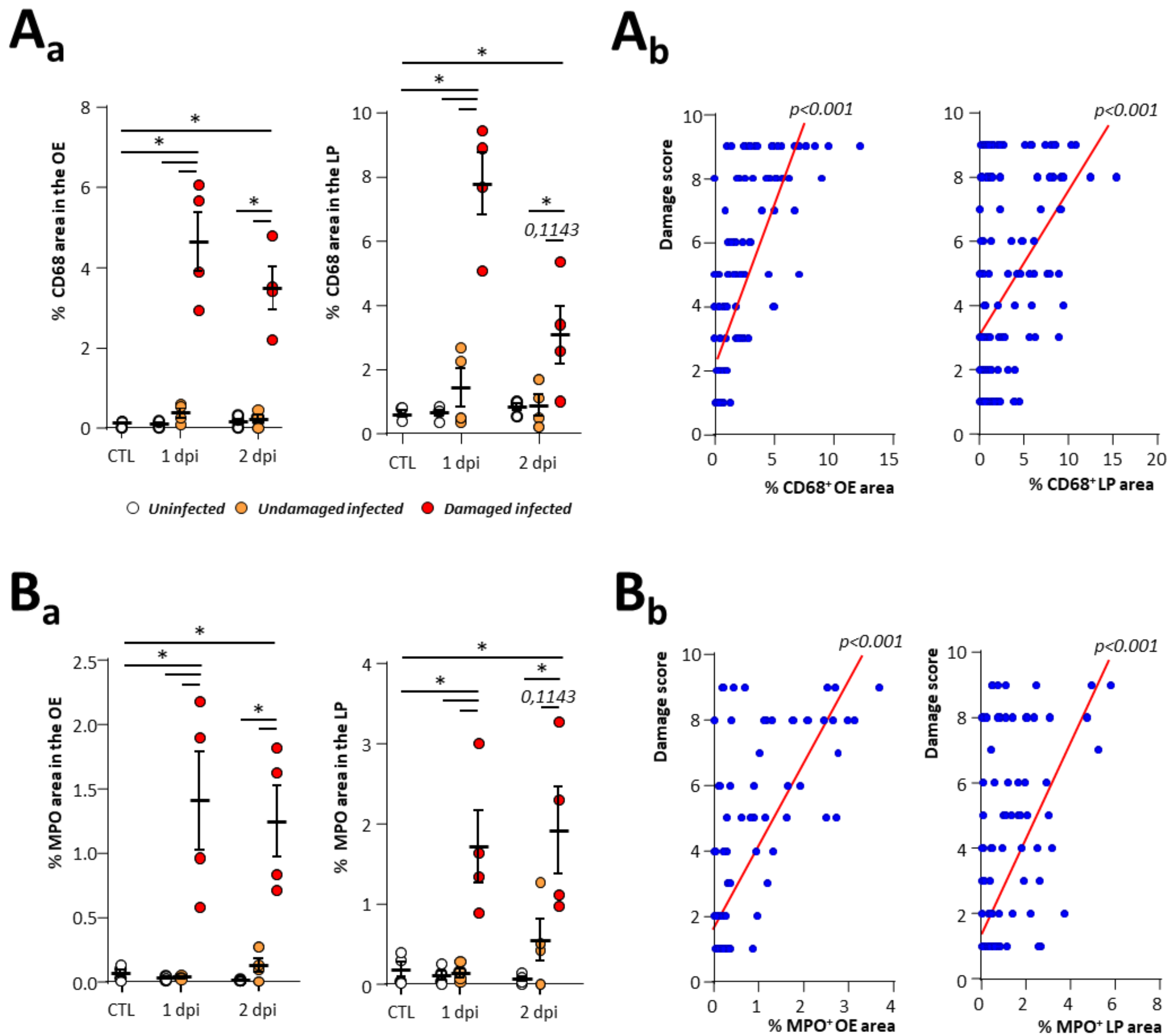

Figure 4: CD68⁺ macrophage and MPO⁺ neutrophil cells are associated with damage of the olfactory epithelium during SARS-CoV-2 infection. *CD68⁺ (**Aa**) and MPO⁺ (**Bb**) signal in the olfactory epithelium (OE, left) and lamina propria (LP, right) in either control animals (CTL) or at 1 or 2-days post infection (dpi) (Mean normalized to control ± SEM, n=4, *p<0.05 (Mann-Whitney test)). Correlation between score damage and percentage of CD68⁺ (**Aa**) and MPO ⁺ (**Bb**) signal in the olfactory epithelium (left panel) and the lamina propria (right panel). Spearman test p value.*

250 **Neutropenia reduces damage of the OE related to SARS-CoV-2 infection as well as level of virus**
251 **infection**

252 Neutrophils are the main actors of damage to the olfactory epithelium during Poly(I:C) induced
253 inflammation (*45*). We therefore evaluated whether a neutropenic treatment based on
254 cyclophosphamide would reduce the damage induced by SARS-CoV-2 infection in the OE. Such
255 treatment causes apoptosis of bone marrow derived cells and has previously been used successfully

bioRxiv preprint doi: https://doi.org/10.1101/2022.03.15.484439; this version posted March 15, 2022. The copyright holder for this preprint (which was not certified by peer review) is the author/funder, who has granted bioRxiv a license to display the preprint in perpetuity. It is made available under aCC-BY-NC-ND 4.0 International license.

256 on hamsters to induce neutropenia (*44*). We first monitored in control animals how the treatment
257 impacts circulating immune cells. Neutrophils population was decreased by ~10-fold, lymphocytes
258 were also decreased by ~3-fold, and monocytes by ~5-fold (**Supp Fig. 3A**). Since cyclophosphamide can
259 impact basal cell proliferation and thus OE structure, we examined its effect in uninfected animals and
260 did not observe any evident damage on the OE structure (**Supp Fig. 3B**). We next examined the impact
261 of this treatment on the expression of genes related to the innate immune system in the nasal
262 turbinates during SARS-CoV-2 infection. At 1 dpi, the expression of Iba1 and CD68 reflecting the
263 population of microglia and monocytes/macrophages respectively was not statistically different
264 between vehicle and cyclophosphamide treated animals but a decrease of Ncf2 expression reflecting
265 a reduced presence of neutrophils almost reached significance (Mann Whitney; $p=0.0571$; **Fig. 6A**). We
266 observed a tendency of TNFα and IL6 expression reduction which did not reach significance either
267 ($p=0.1143$). Despite the overall tendency of a decrease of innate immune system response at 1 dpi,
268 the level of SARS-CoV-2 infection reflected by N protein expression was decreased and the difference
269 almost reached significance ($p=0.0571$). At 2 dpi, the expression of all genes related to innate immune
270 cell presence as well as TNFα were decreased ($p<0.05$). We could not make definitive conclusions
271 about IL6 and SARS-CoV-2 N protein expression because it was very variable in cyclophosphamide
272 treated animals. We examined histologically the damage and the level of infection in the OE (**Fig. 5 B,**
273 **C**). MPO signal was significantly decreased at 1 dpi in the OE of cyclophosphamide treated animals
274 compared to control ($p<0.05$) but was too variable at 2 dpi to reach significance (**Fig. 5 D_a**). The damage
275 in the OE was significantly decreased at 1 and 2 dpi ($p<0.01$ and $p<0.05$ respectively) (**Fig. 5 D_b**). The
276 reduction tendency of the virus presence measured by the N protein expression was confirmed by
277 immunostaining in the OE at 1 dpi only ($p<0.05$; **Fig. 6 D_c**). We hypothesize that this reduction could be
278 linked to less infected desquamated cells released into the lumen of the nasal cavity following the
279 damage induced by the neutrophils. We thus quantified the area of desquamated cells in the lumen
280 which was significantly decreased at 1 dpi and almost reached significance at 2 dpi (**Fig. 5 D_d**; $p<0.001$
281 and $p=0.0905$ respectively). In the desquamated cells of the lumen, the percentage of infected cells
282 was significantly diminished at 1 dpi (**Fig. 5 D_e**; $p<0.001$) but not at 2 dpi when infected desquamated
283 cells were in the lumen of the nasal cavity in some treated animals (**Supp Fig. 3C**). Since the reduction
284 of SARS-CoV-2 replication in the nasal cavity of immunocompromised animal was unexpected, we
285 verified that a dose 3 times higher than the maximum dose of cyclophosphamide potentially present
286 in the hamsters during infection did not limit the virus replication *in vitro* (**Supp Fig. 4A**).

bioRxiv preprint doi: https://doi.org/10.1101/2022.03.15.484439; this version posted March 15, 2022. The copyright holder for this preprint (which was not certified by peer review) is the author/funder, who has granted bioRxiv a license to display the preprint in perpetuity. It is made available under aCC-BY-NC-ND 4.0 International license.

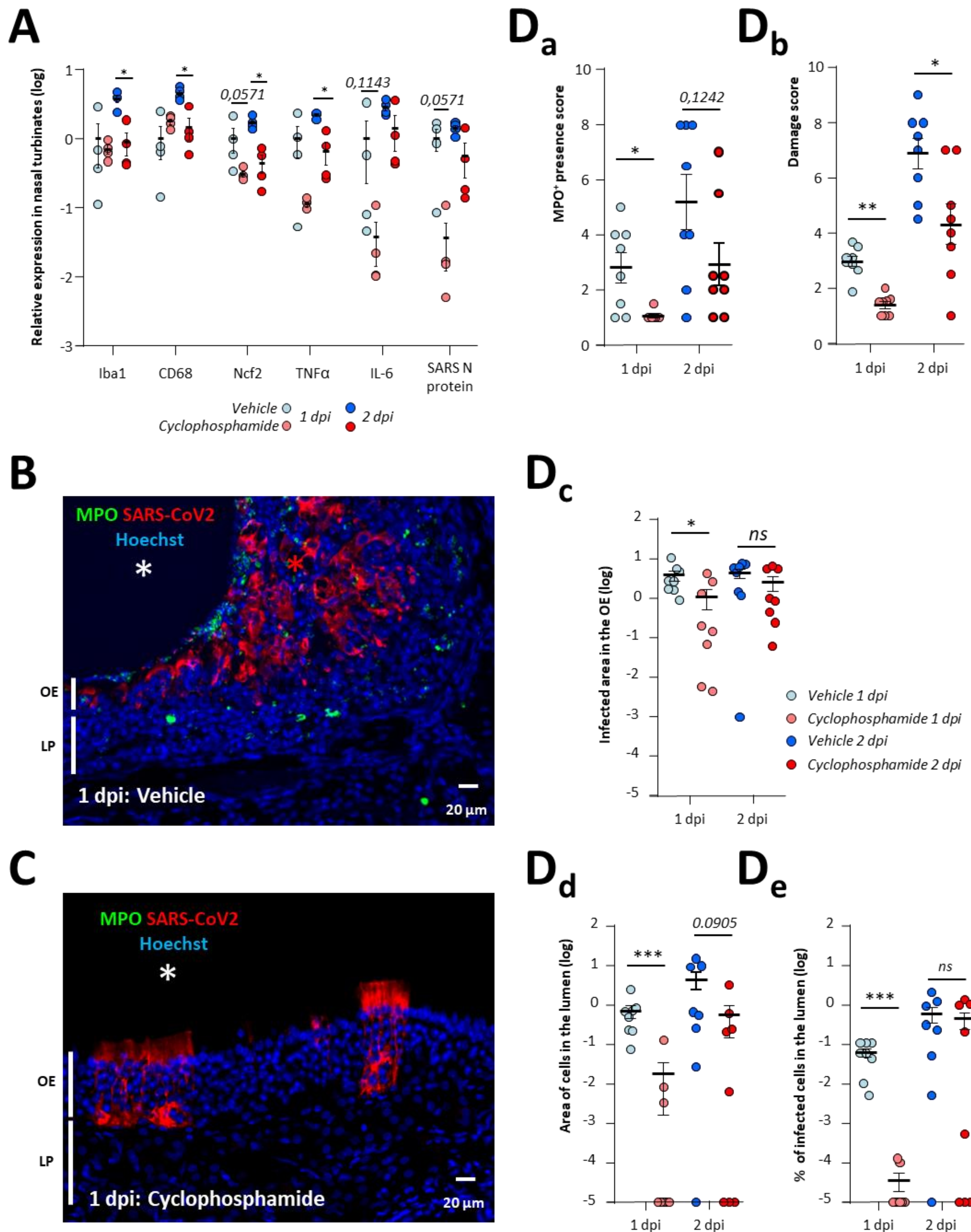

Figure 5: Immunosuppression induced by cyclophosphamide reduces damage of the olfactory epithelium as well as virus replication. *(**A**) Expression of innate immune genes in the nasal turbinates with or without cyclophosphamide treatment at 1 and 2-days post infection (dpi). Iba1, CD68 and Ncf2 are related to the presence of microglia/macrophages, monocytes/macrophages and neutrophils respectively; TNFα and IL6 are two cytokines expressed during inflammation; SARS-CoV-*

bioRxiv preprint doi: https://doi.org/10.1101/2022.03.15.484439; this version posted March 15, 2022. The copyright holder for this preprint (which was not certified by peer review) is the author/funder, who has granted bioRxiv a license to display the preprint in perpetuity. It is made available under aCC-BY-NC-ND 4.0 International license.

*2 N expression is related to the SARS-CoV-2 infection. Results represent the mean ± SEM relative to vehicle treated hamsters (n=4, *p<0.05; Mann-Whitney test). Representative images of the infected olfactory epithelium immunostained for MPO (neutrophil marker) and SARS-CoV-2 N protein in (**B**) vehicle and (**C**) cyclophosphamide treated animal (olfactory epithelium (OE), lamina propria (LP)). In the vehicle condition, the lumen (white asterisk) is filled with desquamated cells (red asterisk) containing MPO signal. In the cyclophosphamide condition, MPO signal is absent and the lumen is mostly free of cellular debris. Quantification in the OE of (**D_1**) MPO^+ neutrophil presence (**D_2**) damage score (**D_3**) SARS-CoV-2 infected area and in the lumen of the nasal cavity of (**D_4**) desquamated cells area and (**D_5**) percentage of SARS-CoV-2 infected area in the desquamated cells (Mean normalized to infected animals treated with vehicle ± SEM, n=8 areas of the nasal cavity from 4 different animals, *p<0.05, **p<0.01, ***p<0.001 (Mann-Whitney)).*

287 **Inhibition of neutrophil proteinases reduces damage of the OE related to SARS-CoV-2 infection as**
288 **well as virus spreading in the nasal cavity**

289 In order to confirm our results on cyclophosphamide treatment which affects immune cells other than
290 neutrophils, we treated animals with an inhibitor of cathepsin C ($IcatC_{XPZ-01}$) which is essential for the
291 maturation of elastase-like proteinases of neutrophils. This inhibitor has been used successfully to
292 almost completely eliminate the elastase-like activity of neutrophils *in vivo* (*38*). We chose to focus on
293 the histological impact of $IcatC_{XPZ-01}$ treatment at 1 dpi as it gave the most significant results during
294 cyclophosphamide treatment. The inhibition of elastase-like proteinases of neutrophils gave similar
295 results as cyclophosphamide treatment even though we sometimes observed locally restricted
296 neutrophil infiltration in the OE (**Fig. 6 A, B**). Globally the MPO^+ neutrophil presence in the nasal
297 turbinates and the damage in the infected area of the OE were significantly reduced compared to
298 vehicle treated animals (**Fig. 6C_1**; Mann-Whitney; *p<0.01*). We also observed significantly less
299 desquamated cells in the lumen of the nasal cavity which were also less infected (**Fig. 6C_2**; Mann-
300 Whitney; *p<0.01*). Since we observed again that the inhibition of neutrophil action limited SARS-CoV-
301 2 replication, we verified that a dose 3 times higher than the maximum dose of $IcatC_{XPZ-01}$ potentially
302 present in the hamsters during infection did not impair the virus replication *in vitro* (**Supp Fig. 4B**).

bioRxiv preprint doi: https://doi.org/10.1101/2022.03.15.484439; this version posted March 15, 2022. The copyright holder for this preprint (which was not certified by peer review) is the author/funder, who has granted bioRxiv a license to display the preprint in perpetuity. It is made available under aCC-BY-NC-ND 4.0 International license.

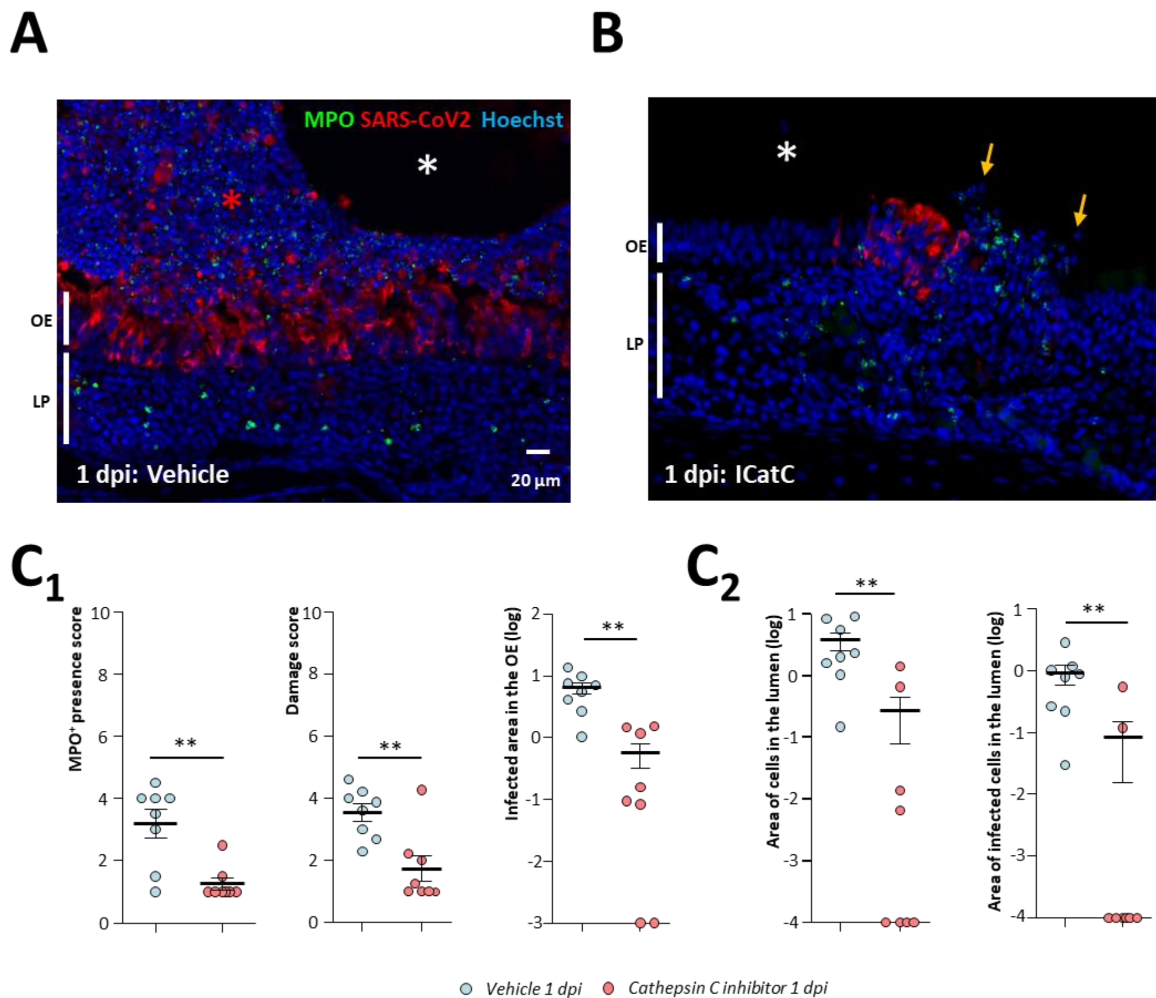

Figure 6: Inhibition of neutrophil proteinases reduces damage of the olfactory epithelium as well as virus spreading in the nasal cavity. *Representative images of the infected olfactory epithelium immunostained for MPO (neutrophil marker) and SARS-CoV-2 N protein in (**A**) vehicle and (**B**) cathepsin C inhibitor (IcatC$_{XPZ\text{-}01}$) treated animal (olfactory epithelium (OE), lamina propria (LP)). In the vehicle condition, the lumen (white asterisk) is filled with desquamated cells (red asterisk) containing MPO signal. Under cathepsin C inhibition, MPO signal is less abundant and the lumen is mostly free of cellular debris (yellow arrows)**.** Quantification **(C_1)** in the OE of MPO$^+$ neutrophil presence; damage score; SARS-CoV-2 infected area and **(C_2)** in the lumen of the nasal cavity of desquamated cell area and percentage of SARS-CoV-2 infected area in the desquamated cells (Mean normalized to infected animals treated with vehicle ± SEM, n=8 areas of the nasal cavity from 4 different animals, *p<0.05, **p<0.01, ***p<0.001 (Mann-Whitney test)).*

303 ## Discussion

304 The anosmia induced by SARS-CoV-2 infection is now clearly linked to the infection of the olfactory
305 epithelium with a main tropism for sustentacular cells (*46*, *47*). We and others have observed that

bioRxiv preprint doi: https://doi.org/10.1101/2022.03.15.484439; this version posted March 15, 2022. The copyright holder for this preprint (which was not certified by peer review) is the author/funder, who has granted bioRxiv a license to display the preprint in perpetuity. It is made available under aCC-BY-NC-ND 4.0 International license.

306 following this infection, the OE undergoes massive damage leading to cell desquamation and cellular
307 debris filling the lumen of the nasal cavity (*13*, *19*, *20*), but the mechanism of this destruction is less
308 clear.

309 Several studies reported an increase of apoptosis especially in olfactory sensory neurons (*18*–*20*) and
310 assumed that it led to the destruction of the OE. Here, we first examined the apoptosis level based on
311 cleaved caspase 3 level in the OE of uninfected animals and infected areas of the OE, either intact or
312 damaged. If apoptosis initiates the desquamation process then it should increase in the damaged areas
313 of the OE. However, we observed a similar level of apoptosis level in all these areas which was
314 consistent with the basal level of apoptosis that we previously measured in adult mice and rats OE (*48*,
315 *49*). While the apoptosis in the infected damaged OE was low, we observed an increased level of
316 apoptosis in cells present in the lumen of the nasal cavity. The discrepancy with previous studies may
317 be due to different models as some were performed using transgenic mice expressing hACE2 but it
318 should be noted that these studies did not perform any quantification or misinterpreted some
319 apoptosis staining in the lumen of the nasal cavity as can be observed with TUNEL staining (*20*) . The
320 induction of apoptosis by loss of cell contact is well described (*50*), a phenomenon known as anoikis
321 (*51*). It indicates that desquamated cells are sufficiently preserved to be able to enter apoptosis after
322 the desquamation process is initiated following OE SARS-CoV-2 infection.

323 Since we previously observed that the infected area of the OE is infiltrated by immune cells (*13*), we
324 next explored whether innate immune cells are involved in this process, especially macrophages and
325 neutrophils known to be involved in damage of epithelial cells during acute inflammation (*28*, *29*). If
326 so, we should systematically observe their presence in the damaged area of the OE. We first
327 characterized the presence of these cells in the infected OE. We observed that CD68, a classical marker
328 of macrophages (*42*) was expressed in a different population than Iba1$^+$ cells previously described as a
329 microglia/macrophages cellular population (*24*). Therefore, in the following, we will refer to Iba1$^+$ cells
330 as microglia, and CD68$^+$ cells as macrophages to avoid confusion between these two cells types.
331 Immunostaining revealed that at 1 dpi, some parts of the OE in the most rostral part of the nasal cavity
332 were already significantly damaged. We observed that in these tissues, microglia cells were mainly
333 recruited while macrophages and neutrophils appeared in the zones desquamating toward the lumen
334 of the nasal cavity. We can thus hypothesize that microglia are first infiltrating the SARS-CoV-2 infected
335 OE. This is not consistent with our qPCR results indicating that neutrophils are recruited more
336 abundantly at 1 dpi than microglia and macrophages. However, we observed that contrary to
337 macrophages and neutrophils, microglia cells were already present in the lamina propria of uninfected
338 zones. At the beginning of infection, the increase of microglia cells could simply arise from infiltration
339 of adjacent cells in the nasal turbinates, while macrophages and neutrophils may migrate from the

bioRxiv preprint doi: https://doi.org/10.1101/2022.03.15.484439; this version posted March 15, 2022. The copyright holder for this preprint (which was not certified by peer review) is the author/funder, who has granted bioRxiv a license to display the preprint in perpetuity. It is made available under aCC-BY-NC-ND 4.0 International license.

340 blood following chemotaxis. Microglia are recruited around infected cells of the central nervous
341 system within hours (Fekete et al., 2018) which is consistent with our observation in the OE. Further
342 studies are required to decipher the origin of these 3 cells population during the early events of SARS-
343 CoV-2 infection in the infected nasal turbinates.

344 Neutrophils are known to induce epithelial damage and an elegant study demonstrated their major
345 role during Poly I:C (an artificial double stranded RNA agonist of TLR3 receptor) nasal instillation
346 leading to damage of the OE (*45*). In order to evaluate the importance of the neutrophils in the damage
347 induced by SARS-CoV-2, we first induced neutropenia based on previous cyclophosphamide treatment
348 successfully used in hamsters (*44*). We confirmed that such treatment mainly impacts neutrophils but
349 also reduced to a lesser degree other leucocyte populations. As expected such treatment reduced
350 neutrophil infiltration in infected areas of the OE and we observed that damage of the infected OE was
351 significantly reduced as well. In order to confirm the role of neutrophils in the damage of the OE
352 following SARS-CoV-2 infection, we treated hamsters with an inhibitor of cathepsin C ($IcatC_{XPZ-01}$)
353 strongly reducing the neutrophil elastase-like proteinases activity. We observed that similar to
354 cyclophosphamide treatment, the damage of the OE was greatly reduced in this context. Surprisingly,
355 the global infiltration of neutrophils was reduced as well, even though we observed that some
356 neutrophils were still present in the most infected area of the OE. Since neutrophils are mainly present
357 among the desquamated cells present in the lumen of the nasal cavity, the reduction in neutrophil
358 infiltration during $IcatC_{XPZ-01}$ treatment may be linked to a decrease of the OE damage as elastase-like
359 proteinase action increases inflammation (*52*). It suggests that the damage of the OE initiated by
360 neutrophils may participate in the increasing infiltration of neutrophils leading *in fine* to massive
361 damage of the infected OE areas. Overall, these results show that neutrophils have a major causative
362 role in the destruction of the OE following SARS-CoV-2 infection by releasing elastase-like proteinases.

363 We observed that at 1 dpi, the level of SARS-CoV-2 infection was reduced in cyclophosphamide and
364 $IcatC_{XPZ-01}$ treated hamsters. Such a result was unexpected as neutrophils should effectively destroy
365 infected cells and thus their action should reduce infection progression. Since we observed that these
366 treatments did not impair SARS-CoV-2 replication *in vitro*, we hypothesize that neutrophils may have
367 a counterproductive effect by releasing infected cells into the lumen of the nasal cavity. These infected
368 cells could allow the virus to spread more easily in the nasal cavity due to impairment of mucociliary
369 clearance that has been recently shown to be reduced during SARS-CoV-2 infection (*53*). Such a
370 hypothesis is consistent with our results showing that cyclophosphamide and $IcatC_{XPZ-01}$ treatment
371 significantly reduced the amount of infected desquamated cells filling the lumen of the nasal cavity.
372 Such a phenomenon has been observed recently *in vitro* in respiratory epithelial cell culture where
373 infection is enhanced in the presence of neutrophils. In their preliminary study, SARS-CoV-2 alone did

bioRxiv preprint doi: https://doi.org/10.1101/2022.03.15.484439; this version posted March 15, 2022. The copyright holder for this preprint (which was not certified by peer review) is the author/funder, who has granted bioRxiv a license to display the preprint in perpetuity. It is made available under aCC-BY-NC-ND 4.0 International license.

374 not significantly increase cytokine production but the neutrophil presence did, showing a major role
375 of the neutrophils in the epithelial response to SARS-CoV-2 infection (*54*). At 2 dpi, the impact of
376 neutropenia on SARS-CoV-2 infection in the nasal cavity was statistically significant through the
377 reduction of OE damage. The neutropenia induced by the cyclophosmamide treatment was only
378 partial, we can thus hypothesize that the remaining neutrophils can be more effectively recruited when
379 infection progresses and thus we could no longer observe a statistically significant decrease of
380 neutrophil infiltration and SARS-CoV-2 infection in the OE.

381 Overall, our results show that the SARS-CoV-2 infection does not directly induce the massive damage
382 of the OE but that neutrophils play a major role by releasing elastase-like proteinase in the infected
383 OE. This probably leads to the destabilisation of the OE structures and the expulsion of cells including
384 non-infected neurons into the lumen of the nasal cavity where they would undergo apoptosis. In the
385 early phase of the infection, such expulsion of infected cells could enhance the virus infection in the
386 nasal cavity (**Fig. 7**). We observed damaged areas of the OE as soon as 1 dpi indicating that the innate
387 immune system is extremely efficient in detecting SARS-CoV-2 infected cells to destroy them. The
388 signal triggering this very fast action remains to be explored. The host's immune defence system that
389 may be present to prevent pathogen invasion from the nose to the brain seems beneficial for SARS-
390 CoV-2 to achieve a much more extensive infection of the OE than any previous virus, resulting in
391 unprecedented olfactory dysfunction in the COVID-19 pandemic.

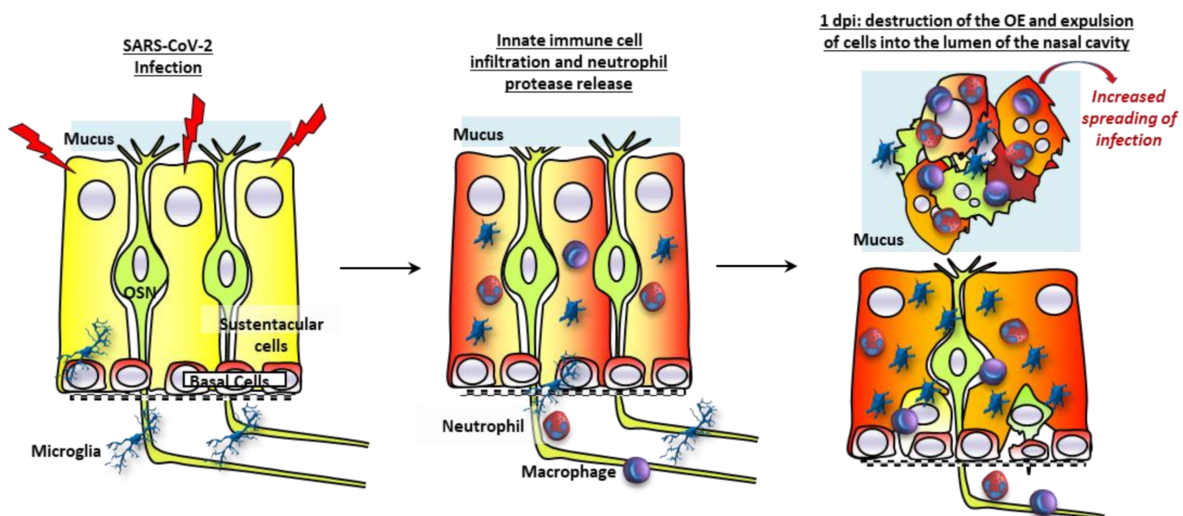

Figure 7: Model of innate immune cell signalling leading to olfactory epithelium desquamation. *The olfactory epithelium is mainly composed of olfactory sensory neurons (OSN) surrounded by supporting cells (sustentacular cells) and basal cells able to regenerate all cell types of the epithelium. During the infection of sustentacular cells (turning red), microglia become activated and infiltrate the olfactory epithelium followed by neutrophils and macrophages. Neutrophils release elastase-like*

bioRxiv preprint doi: https://doi.org/10.1101/2022.03.15.484439; this version posted March 15, 2022. The copyright holder for this preprint (which was not certified by peer review) is the author/funder, who has granted bioRxiv a license to display the preprint in perpetuity. It is made available under aCC-BY-NC-ND 4.0 International license.

proteinase leading to destabilization of the epithelium structures and the expulsion of cells including non-infected neurons into the lumen of the nasal cavity. These desquamated cells – after losing cell contact – undergo apoptosis with a nuclear fragmentation. The release of infected cells may contribute to an increased spreading of the virus in the nasal cavity.

392 **Supplementary materials:**

393 **Supplementary Table 1**: Sequences of primers

394 **Supplementary Figure 1:** Expression of different genes in the nasal turbinates during SARS-CoV-2
395 infection

396 **Supplementary Figure 2**: Double staining against Iba1 and CD68 markers in the desquamated cells
397 filling the lumen of the nasal cavity

398 **Supplementary Figure 3**: Blood numeration, impact on OE structure and representative images of
399 the nasal cavity at 2 dpi during cyclophosphamide treatment.

400 **Supplementary Figure 4**: Impact of cyclophosphamide and cathepsin C inhibitor on virus replication
401 *in vitro*.

402 **Acknowledgment:** We would like to thank all VIM members for their helpful discussion, Christopher
403 von Bartheld and Birte Nielsen for improvement of the manuscript, Dr Pierre Deshuillers from the
404 BioPole plateform of the National Veterinary School of Alfort for hamsters' blood count, all the people
405 from the PRBM plateform of ENVA who helped us in the BSL3 animal facility. Bertrand Bryche, Georges
406 Saade, Mustapha Si-Tahar and Déborah Diakite for helpful discussion and technical help. **Funding**: NM
407 is supported by INRAe SA department and ANR (Grant CORAR). BK is supported by the "Région Centre
408 Val de Loire (Project Pirana). **Authors contribution:** Conceptualization NM and CB Investigation: CB,
409 ASA, OAG, BDC, RD, BK, BK, SLP, NM Formal analysis: CB and NM Writing: NM and CB with input from
410 all authors. **Competing interests:** All authors do not have conflict of interest

bioRxiv preprint doi: https://doi.org/10.1101/2022.03.15.484439; this version posted March 15, 2022. The copyright holder for this preprint (which was not certified by peer review) is the author/funder, who has granted bioRxiv a license to display the preprint in perpetuity. It is made available under aCC-BY-NC-ND 4.0 International license.

411 **References:**

412 1. von Bartheld CS, M. M. Hagen, R. Butowt, Prevalence of Chemosensory Dysfunction in COVID-
413 19 Patients: A Systematic Review and Meta-analysis Reveals Significant Ethnic Differences. *ACS*
414 *Chemical Neuroscience* (2020), doi:10.1021/acschemneuro.0c00460.

415 2. L. A. Vaira, A. De Vito, J. R. Lechien, C. M. Chiesa-Estomba, M. Mayo-Yàñez, C. Calvo-Henrìquez,
416 S. Saussez, G. Madeddu, S. Babudieri, P. Boscolo-Rizzo, C. Hopkins, G. De Riu, *The Laryngoscope*,
417 in press, doi:10.1002/lary.29964.

418 3. P. Boscolo-Rizzo, A. Menegaldo, C. Fabbris, G. Spinato, D. Borsetto, L. A. Vaira, L. Calvanese, A.
419 Pettorelli, M. Sonego, D. Frezza, A. Bertolin, W. Cestaro, R. Rigoli, A. D'Alessandro, G. Tirelli, M.
420 C. Da Mosto, A. Menini, J. Polesel, C. Hopkins, Six-month psychophysical evaluation of olfactory
421 dysfunction in patients with COVID-19. *Chem Senses* (2021), doi:10.1093/chemse/bjab006.

422 4. J. R. Lechien, C. M. Chiesa-Estomba, E. Beckers, V. Mustin, M. Ducarme, F. Journe, A. Marchant,
423 L. Jouffe, M. R. Barillari, G. Cammaroto, M. P. Circiu, S. Hans, S. Saussez, Prevalence and 6-
424 month recovery of olfactory dysfunction: a multicentre study of 1363 COVID-19 patients.
425 *Journal of internal medicine* (2021), doi:10.1111/joim.13209.

426 5. M. Renaud, C. Thibault, F. Le Normand, E. G. Mcdonald, B. Gallix, C. Debry, A. Venkatasamy,
427 Clinical Outcomes for Patients With Anosmia 1 Year After COVID-19 Diagnosis. *JAMA Netw*
428 *Open*. **4**, e2115352 (2021).

429 6. A. M. Khan, D. Kallogjeri, J. F. Piccirillo, Growing Public Health Concern of COVID-19 Chronic
430 Olfactory Dysfunction. *JAMA Otolaryngol Head Neck Surg* (2021),
431 doi:10.1001/jamaoto.2021.3379.

432 7. N. Meunier, L. Briand, A. Jacquin-Piques, L. Brondel, L. Pénicaud, COVID 19-Induced Smell and
433 Taste Impairments: Putative Impact on Physiology. *Frontiers in physiology*. **11** (2021),
434 doi:10.3389/fphys.2020.625110.

435 8. H. Rebholz, R. J. Braun, D. Ladage, W. Knoll, C. Kleber, A. W. Hassel, Loss of Olfactory Function-
436 Early Indicator for Covid-19, Other Viral Infections and Neurodegenerative Disorders. *Frontiers*
437 *in neurology*. **11**, 569333 (2020).

438 9. J. E. Schwob, W. Jang, E. H. Holbrook, B. Lin, D. B. Herrick, J. N. Peterson, J. Hewitt Coleman,
439 Stem and progenitor cells of the mammalian olfactory epithelium: Taking poietic license. *J*
440 *Comp Neurol*. **525**, 1034–1054 (2017).

441 10. K. Bilinska, P. Jakubowska, V. O. N. Bartheld CS, R. Butowt, Expression of the SARS-CoV-2 Entry
442 Proteins, ACE2 and TMPRSS2, in Cells of the Olfactory Epithelium: Identification of Cell Types
443 and Trends with Age. *ACS Chemical Neuroscience* (2020), doi:10.1021/acschemneuro.0c00210.

444 11. D. H. Brann, T. Tsukahara, C. Weinreb, M. Lipovsek, K. Van den Berge, B. Gong, R. Chance, I. C.
445 Macaulay, H.-J. Chou, R. B. Fletcher, D. Das, K. Street, H. R. de Bezieux, Y.-G. Choi, D. Risso, S.
446 Dudoit, E. Purdom, J. Mill, R. A. Hachem, H. Matsunami, D. W. Logan, B. J. Goldstein, M. S.
447 Grubb, J. Ngai, S. R. Datta, Non-neuronal expression of SARS-CoV-2 entry genes in the olfactory
448 system suggests mechanisms underlying COVID-19-associated anosmia. *Sci. Adv.* **6**, eabc5801
449 (2020).

bioRxiv preprint doi: https://doi.org/10.1101/2022.03.15.484439; this version posted March 15, 2022. The copyright holder for this preprint (which was not certified by peer review) is the author/funder, who has granted bioRxiv a license to display the preprint in perpetuity. It is made available under aCC-BY-NC-ND 4.0 International license.

450 12. L. Fodoulian, J. Tuberosa, D. Rossier, M. Boillat, C. Kan, V. Pauli, K. Egervari, J. A. Lobrinus, B. N.
451 Landis, A. Carleton, I. Rodriguez, SARS-CoV-2 receptors and entry genes are expressed in the
452 human olfactory neuroepithelium and brain. *iScience*, 101839 (2020).

453 13. B. Bryche, A. St Albin, S. Murri, S. Lacote, C. Pulido, M. Ar Gouilh, S. Lesellier, A. Servat, M.
454 Wasniewski, E. Picard-Meyer, E. Monchatre-Leroy, R. Volmer, O. Rampin, R. Le Goffic, P.
455 Marianneau, N. Meunier, Massive transient damage of the olfactory epithelium associated with
456 infection of sustentacular cells by SARS-CoV-2 in golden Syrian hamsters. *Brain, behavior, and*
457 *immunity*. **89**, 579–586 (2020).

458 14. S. Urata, M. Kishimoto-Urata, R. Kagoya, F. Imamura, S. Nagayama, R. A. Reyna, J. Maruyama, T.
459 Yamasoba, K. Kondo, S. Hasegawa-Ishii, S. Paessler, *bioRxiv*, in press,
460 doi:10.1101/2021.11.04.467274.

461 15. R. Butowt, N. Meunier, B. Bryche, C. S. von Bartheld, The olfactory nerve is not a likely route to
462 brain infection in COVID-19: a critical review of data from humans and animal models. *Acta*
463 *neuropathologica*. **141**, 809–822 (2021).

464 16. J. W. Harding, T. V. Getchell, F. L. Margolis, Denervation of the primary olfactory pathway in
465 mice. V. Long-term effect of intranasal ZnSO4 irrigation on behavior, biochemistry and
466 morphology. *Brain Research*. **140**, 271–285 (1978).

467 17. J. S. Seo, S. W. Yoon, S. H. Hwang, S. M. Nam, S. S. Nahm, J. H. Jeong, J. Lee, H. N. Youn, J. B.
468 Kim, W. Kim, The Microvillar and Solitary Chemosensory Cells as the Novel Targets of Infection
469 of SARS-CoV-2 in Syrian Golden Hamsters. *Viruses*. **13** (2021), doi:10.3390/v13081653.

470 18. Q. Ye, J. Zhou, Q. He, R. T. Li, G. Yang, Y. Zhang, S. J. Wu, Q. Chen, J. H. Shi, R. R. Zhang, H. M.
471 Zhu, H. Y. Qiu, T. Zhang, Y. Q. Deng, X. F. Li, J. F. Liu, P. Xu, X. Yang, C. F. Qin, SARS-CoV-2
472 infection in the mouse olfactory system. *Cell discovery*. **7**, 49 (2021).

473 19. P. Yu, W. Deng, L. Bao, Y. Qu, Y. Xu, W. Zhao, Y. Han, C. Qin, Comparative pathology of the nasal
474 epithelium in K18-hACE2 Tg mice, hACE2 Tg mice, and hamsters infected with SARS-CoV-2. *Vet*
475 *Pathol*, 030098582110710 (2022).

476 20. A. J. Zhang, A. C.-Y. Lee, H. Chu, J. F.-W. Chan, Z. Fan, C. Li, F. Liu, Y. Chen, S. Yuan, V. K.-M.
477 Poon, C. C.-S. Chan, J.-P. Cai, K. L.-K. Wu, S. Sridhar, Y.-S. Chan, K.-Y. Yuen, Severe Acute
478 Respiratory Syndrome Coronavirus 2 Infects and Damages the Mature and Immature Olfactory
479 Sensory Neurons of Hamsters. *Clinical Infectious Diseases*. **73**, e503–e512 (2021).

480 21. I. Mori, F. Goshima, Y. Imai, S. Kohsaka, T. Sugiyama, T. Yoshida, T. Yokochi, Y. Nishiyama, Y.
481 Kimura, Olfactory receptor neurons prevent dissemination of neurovirulent influenza A virus
482 into the brain by undergoing virus-induced apoptosis. *The Journal of general virology*. **83**, 2109–
483 16 (2002).

484 22. S. D. Le Bon, M. Horoi, Is anosmia the price to pay in an immune-induced scorched-earth policy
485 against COVID-19? *Medical hypotheses*. **143**, 109881 (2020).

486 23. R. A. Burgoyne, A. J. Fisher, L. A. Borthwick, The Role of Epithelial Damage in the Pulmonary
487 Immune Response. *Cells*. **10**, 2763 (2021).

488 24. Y. Imai, I. Ibata, D. Ito, K. Ohsawa, S. Kohsaka, A Novel Geneiba1in the Major Histocompatibility
489 Complex Class III Region Encoding an EF Hand Protein Expressed in a Monocytic Lineage.
490 *Biochemical and Biophysical Research Communications*. **224**, 855–862 (1996).

bioRxiv preprint doi: https://doi.org/10.1101/2022.03.15.484439; this version posted March 15, 2022. The copyright holder for this preprint (which was not certified by peer review) is the author/funder, who has granted bioRxiv a license to display the preprint in perpetuity. It is made available under aCC-BY-NC-ND 4.0 International license.

491 25. R. Fekete, C. Cserép, N. Lénárt, K. Tóth, B. Orsolits, B. Martinecz, E. Méhes, B. Szabó, V.
492 Németh, B. Gönci, B. Sperlágh, Z. Boldogkői, Á. Kittel, M. Baranyi, S. Ferenczi, K. Kovács, G.
493 Szalay, B. Rózsa, C. Webb, G. G. Kovacs, T. Hortobágyi, B. L. West, Z. Környei, Á. Dénes,
494 Microglia control the spread of neurotropic virus infection via P2Y12 signalling and recruit
495 monocytes through P2Y12-independent mechanisms. *Acta Neuropathol*. **136**, 461–482 (2018).

496 26. D. L. Wheeler, A. Sariol, D. K. Meyerholz, S. Perlman, Microglia are required for protection
497 against lethal coronavirus encephalitis in mice. *J Clin Invest*. **128**, 931–943 (2018).

498 27. C. Käufer, C. Chhatbar, S. Bröer, I. Waltl, L. Ghita, I. Gerhauser, U. Kalinke, W. Löscher,
499 Chemokine receptors CCR2 and CX3CR1 regulate viral encephalitis-induced hippocampal
500 damage but not seizures. *Proc Natl Acad Sci USA*. **115**, E8929–E8938 (2018).

501 28. E. Kolaczkowska, P. Kubes, Neutrophil recruitment and function in health and inflammation.
502 *Nat Rev Immunol*. **13**, 159–175 (2013).

503 29. S. Meidaninikjeh, N. Sabouni, H. Z. Marzouni, S. Bengar, A. Khalili, R. Jafari, Monocytes and
504 macrophages in COVID-19: Friends and foes. *Life Sciences*. **269**, 119010 (2021).

505 30. A. Janoff, Human granulocyte elastase. Further delineation of its role in connective tissue
506 damage. *Am J Pathol*. **68**, 579–592 (1972).

507 31. K. Kawabata, T. Hagio, S. Matsuoka, The role of neutrophil elastase in acute lung injury.
508 *European Journal of Pharmacology*. **451**, 1–10 (2002).

509 32. V. Brinkmann, U. Reichard, C. Goosmann, B. Fauler, Y. Uhlemann, D. S. Weiss, Y. Weinrauch, A.
510 Zychlinsky, Neutrophil Extracellular Traps Kill Bacteria. *Science*. **303**, 1532–1535 (2004).

511 33. M. Saffarzadeh, C. Juenemann, M. A. Queisser, G. Lochnit, G. Barreto, S. P. Galuska, J.
512 Lohmeyer, K. T. Preissner, Neutrophil Extracellular Traps Directly Induce Epithelial and
513 Endothelial Cell Death: A Predominant Role of Histones. *PLoS ONE*. **7**, e32366 (2012).

514 34. G. Arango Duque, A. Descoteaux, Macrophage Cytokines: Involvement in Immunity and
515 Infectious Diseases. *Front. Immunol.* **5** (2014), doi:10.3389/fimmu.2014.00491.

516 35. A. S. Borders, M. L. Getchell, J. T. Etscheidt, N. van Rooijen, D. A. Cohen, T. V. Getchell,
517 Macrophage depletion in the murine olfactory epithelium leads to increased neuronal death
518 and decreased neurogenesis. *J Comp Neurol*. **501**, 206–18 (2007).

519 36. A. S. Borders, M. A. Hersh, M. L. Getchell, N. van Rooijen, D. A. Cohen, A. J. Stromberg, T. V.
520 Getchell, Macrophage-mediated neuroprotection and neurogenesis in the olfactory epithelium.
521 *Physiological genomics*. **31**, 531–43 (2007).

522 37. B. Korkmaz, A. Lesner, M. Wysocka, A. Gieldon, M. Hakansson, F. Gauthier, D. T. Logan, D. E.
523 Jenne, C. Lauritzen, J. Pedersen, Structure-based design and in vivo anti-arthritic activity
524 evaluation of a potent dipeptidyl cyclopropyl nitrile inhibitor of cathepsin C. *Biochemical*
525 *pharmacology*. **164**, 349–367 (2019).

526 38. C. Guarino, Y. Hamon, C. Croix, A. S. Lamort, S. Dallet-Choisy, S. Marchand-Adam, A. Lesner, T.
527 Baranek, M. C. Viaud-Massuard, C. Lauritzen, J. Pedersen, N. Heuze-Vourc'h, M. Si-Tahar, E.
528 Firatli, D. E. Jenne, F. Gauthier, M. S. Horwitz, N. Borregaard, B. Korkmaz, Prolonged
529 pharmacological inhibition of cathepsin C results in elimination of neutrophil serine proteases.
530 *Biochemical pharmacology*. **131**, 52–67 (2017).

bioRxiv preprint doi: https://doi.org/10.1101/2022.03.15.484439; this version posted March 15, 2022. The copyright holder for this preprint (which was not certified by peer review) is the author/funder, who has granted bioRxiv a license to display the preprint in perpetuity. It is made available under aCC-BY-NC-ND 4.0 International license.

531 39. B. Bryche, M. Fretaud, A. Saint-Albin Deliot, M. Galloux, L. Sedano, C. Langevin, D. Descamps,
532 M. A. Rameix-Welti, J. F. Eleouet, R. Le Goffic, N. Meunier, Respiratory syncytial virus tropism
533 for olfactory sensory neurons in mice. *Journal of Neurochemistry*, e14936 (2019).

534 40. P. Y. Muller, H. Janovjak, A. R. Miserez, Z. Dobbie, Processing of gene expression data generated
535 by quantitative real-time RT-PCR. *Biotechniques*. **32**, 1372–1374, 1376, 1378–1379 (2002).

536 41. T. Bouchery, N. Harris, Neutrophil–macrophage cooperation and its impact on tissue repair.
537 *Immunol Cell Biol*. **97**, 289–298 (2019).

538 42. C. Holness, D. Simmons, Molecular cloning of CD68, a human macrophage marker related to
539 lysosomal glycoproteins. *Blood*. **81**, 1607–1613 (1993).

540 43. T. L. Leto, K. J. Lomax, B. D. Volpp, H. Nunoi, J. M. G. Sechler, W. M. Nauseef, R. A. Clark, J. I.
541 Gallin, H. L. Malech, Cloning of a 67-kD Neutrophil Oxidase Factor with Similarity to a
542 Noncatalytic Region of p60 $^{c\text{-}src}$. *Science*. **248**, 727–730 (1990).

543 44. A. G. Peniche, D. L. Bonilla, G. I. Palma, P. C. Melby, B. L. Travi, E. Y. Osorio, A secondary wave of
544 neutrophil infiltration causes necrosis and ulceration in lesions of experimental American
545 cutaneous leishmaniasis. *PLoS One*. **12**, e0179084 (2017).

546 45. K. Kanaya, K. Kondo, K. Suzukawa, T. Sakamoto, S. Kikuta, K. Okada, T. Yamasoba, Innate
547 immune responses and neuroepithelial degeneration and regeneration in the mouse olfactory
548 mucosa induced by intranasal administration of Poly(I:C). *Cell Tissue Res*. **357**, 279–99 (2014).

549 46. V. Fumagalli, M. Ravà, D. Marotta, P. Di Lucia, C. Laura, E. Sala, M. Grillo, E. Bono, L. Giustini, C.
550 Perucchini, M. Mainetti, A. Sessa, J. M. Garcia-Manteiga, L. Donnici, L. Manganaro, S. Delbue, V.
551 Broccoli, R. De Francesco, P. D'Adamo, M. Kuka, L. G. Guidotti, M. Iannacone, Administration of
552 aerosolized SARS-CoV-2 to K18-hACE2 mice uncouples respiratory infection from fatal
553 neuroinvasion. *Sci. Immunol.* **7**, eabl9929 (2022).

554 47. M. Khan, S.-J. Yoo, M. Clijsters, W. Backaert, A. Vanstapel, K. Speleman, C. Lietaer, S. Choi, T. D.
555 Hether, L. Marcelis, A. Nam, L. Pan, J. W. Reeves, P. Van Bulck, H. Zhou, M. Bourgeois, Y.
556 Debaveye, P. De Munter, J. Gunst, M. Jorissen, K. Lagrou, N. Lorent, A. Neyrinck, M.
557 Peetermans, D. R. Thal, C. Vandenbriele, J. Wauters, P. Mombaerts, L. Van Gerven, Visualizing
558 in deceased COVID-19 patients how SARS-CoV-2 attacks the respiratory and olfactory mucosae
559 but spares the olfactory bulb. *Cell*, S0092867421012824 (2021).

560 48. B. Bryche, A. Dewaele, A. Saint-Albin, C. Le Poupon Schlegel, P. Congar, N. Meunier, IL-17c is
561 involved in olfactory mucosa responses to Poly(I:C) mimicking virus presence. *Brain, behavior,*
562 *and immunity* (2019), doi:10.1016/j.bbi.2019.02.012.

563 49. A. Raynaud, N. Meunier, A. Acquistapace, V. Bombail, Chronic variable stress exposure in male
564 Wistar rats affects the first step of olfactory detection. *Behav Brain Res*. **291**, 36–45 (2015).

565 50. R. C. Bates, A. Buret, D. F. van Helden, M. A. Horton, G. F. Burns, Apoptosis induced by
566 inhibition of intercellular contact. *Journal of Cell Biology*. **125**, 403–415 (1994).

567 51. M. Taddei, E. Giannoni, T. Fiaschi, P. Chiarugi, Anoikis: an emerging hallmark in health and
568 diseases. *J. Pathol.* **226**, 380–393 (2012).

569 52. G. Döring, The Role of Neutrophil Elastase in Chronic Inflammation. *Am J Respir Crit Care Med*.
570 **150**, S114–S117 (1994).

bioRxiv preprint doi: https://doi.org/10.1101/2022.03.15.484439; this version posted March 15, 2022. The copyright holder for this preprint (which was not certified by peer review) is the author/funder, who has granted bioRxiv a license to display the preprint in perpetuity. It is made available under aCC-BY-NC-ND 4.0 International license.

571 53. Q. Li, K. Vijaykumar, S. E. Philips, S. S. Hussain, V. N. Huynh, C. M. Fernandez-Petty, J. E. P. Lever,
572 J. B. Foote, J. Ren, J. Campos-Gómez, F. A. Daya, N. W. Hubbs, H. Kim, E. Onuoha, E. R. Boitet, L.
573 Fu, H. M. Leung, L. Yu, T. W. Detchemendy, L. T. Schaefers, J. L. Tipper, L. J. Edwards, S. M. Leal,
574 K. S. Harrod, G. J. Tearney, S. M. Rowe, "Mucociliary Transport Deficiency and Disease
575 Progression in Syrian Hamsters with SARS-CoV-2 Infection" (preprint, Microbiology, 2022), ,
576 doi:10.1101/2022.01.16.476016.

577 54. B. Calvert, E. Quiroz, Z. Lorenzana, N. Doan, S. Kim, C. Senger, W. Wallace, M. Salomon, J.
578 Henley, A. Ryan, "Neutrophil-epithelial interactions augment infectivity and pro-inflammatory
579 responses to SARS-CoV-2 infection" (preprint, Cell Biology, 2021), ,
580 doi:10.1101/2021.08.09.455472.